An Underwater Acoustic OFDM System Based on NI CompactDAQ and LabVIEW

Peng Chen, Yue Rong, *Senior Member, IEEE*, Sven Nordholm, *Senior Member, IEEE*, and Zhiqiang He, *Member, IEEE*

***Abstract*—Recently the orthogonal frequency-division multiplexing (OFDM) technique has attracted increasing interests in underwater acoustic (UA) communications. In this paper, we present an OFDM-based UA communication system, which is designed based on the National Instruments LabVIEW software and the CompactDAQ device. Details on both the transmitter and receiver system design are discussed. The performance of this UA OFDM system is verified through recent UA communication experiments performed in a tank, in the Canning River, and in the estuary of the Swan River, Western Australia. Experimental results show that the system achieves a reliable bit-error-rate performance even with high-order modulation schemes. Compared with conventional field-programmable gate array and digital signal processor based designs, the proposed implementation simplifies the prototype design process and reduces the software development time. The proposed system provides a flexible and reconfigurable prototype for researchers to test and validate the performance of UA communication algorithms in real UA channels.**

***Index Terms*—Underwater acoustic communication, OFDM, LabVIEW, CompactDAQ**

I. Introduction

Underwater acoustic (UA) channels, particularly the shallow water UA channels, are known as the most challenging channels for wireless communication, because of their severe fading, extremely limited bandwidth, significant Doppler shifts, and strong multipath interference [1]. Recently, the orthogonal frequency-division multiplexing (OFDM) technique has been adopted in UA communication thanks to its remarkable capability in mitigating multipath interference with a low computational complexity [2]-[9].

A few UA modems were designed in the research community. In [10] and [11], non-coherent frequency-shift keying (FSK) modems were developed. An acoustic modem based on the spread spectrum technology with Walsh/m-sequence was implemented in [12] using the Texas Instruments C6713 digital signal processor (DSP). A two-mode modem was designed in [13] using a fixed-point DSP, where the non-coherent FSK modulation mode was used for low-power transmission and the coherent phase-shift keying (PSK) mode was applied for high-rate scenarios. A reconfigurable modem was designed in [14] and [15] to simplify the experimental studies of new UA sensor network algorithms on all layers. This modem provides a unified simulation and rapid prototyping environment by transferring the Simulink code into DSP code based on the C6713 DSP Starter Kit. In [16] and [17], OFDM-based UA communication modems implemented through the TMS320C6713 DSP development board were demonstrated. A UA modem based on a DSP-board and an ARM-based BeagleBone board was presented in [18]. The authors of [19] developed a reconfigurable UA modem based on a Xilinx Zynq Z-7020 system-on-chip architecture incorporating a dual ARM Cortex-A9 and an Avnet PicoZed XC7Z020-1CLG400 field-programmable gate array (FPGA). A comprehensive review of existing literature on software-defined modems for UA communications is provided in a recent work [20]. We would like to note that these DSP and FPGA based implementations can be time-consuming on system hardware and software design and implementation [20].

In this paper, a National Instruments (NI) LabVIEW and CompactDAQ-based design of UA OFDM transceiver prototype running on general-purpose processors (GPPs) is presented. Details on both the transmitter and receiver system design are discussed. In this prototype system, the receiver immediately starts to process the signals once they are received, and the receiver is able to complete processing one data frame before the end of the next data frame in a continuous fashion.

Compared with DSP and FPGA based designs [12]-[20], the proposed implementation is more flexible and has a shorter development time. In general, a thorough knowledge of the specific hardware and/or software architecture is needed to modify a UA modem implemented on a dedicated architecture, such as a DSP or FPGA. On the contrary, there is less specialized knowledge required on our system as it is running on GPPs. Using our system, researchers are relived from programming a dedicated processor such as a DSP, which enables them to focus their efforts in developing high-performance UA communication algorithms. Although some of the systems in [20] are GPP-based, they do not exploit the convenient graphical programming environment of LabVIEW. Moreover, LabVIEW provides simplified integration with hardware which enables a rapid system configuration. In general, a NI LabVIEW-based transceiver running on GPPs has a larger power consumption than a DSP-based modem. This is a trade-off for the flexibility of our system. Our system provides researchers a flexible and

This work was supported by the Australian Research Council's Discovery Projects funding scheme (DP140102131) and the National Natural Science Foundation of China under Grant 61671080. Part of this work has been presented at the 23rd Asia-Pacific Conference on Communications, Perth, Australia, Dec. 2017.

P. Chen, Y. Rong, and S. Nordholm are with the School of Electrical Engineering, Computing and Mathematical Sciences, Curtin University, Bentley, WA, Australia (e-mails: peng.ch@outlook.com; y.rong@curtin.edu.au; s.nordholm@curtin.edu.au).

Z. He is with the Key Laboratory of Universal Wireless Communication, Ministry of Education, Beijing University of Posts and Telecommunications, Beijing 100876, China (e-mail: hezq@bupt.edu.cn).

reconfigurable UA communication transceiver to test the performance of their algorithms. With the graphical programming environment of LabVIEW, researchers can easily integrate their UA communication algorithms into our system, quickly test and validate their algorithms in real UA channels, and efficiently improve the performance of their algorithms based on the experimental results. Once these algorithms are mature for commercial/practical deployment, they can be ported into DSP or FPGA.

Thanks to the well-designed toolbox functions, MATLAB is good at complex signal processing tasks. However in many scenarios, LabVIEW codes run faster than Matlab. In [21], the same set of system algorithms are implemented using equivalent codes from LabVIEW and MATLAB, respectively, to carry out a fair and objective one-to-one comparison. It is reported in [21] that the LabVIEW simulator outperforms the MATLAB simulator by a factor of ten in computational time. In [22], it is shown that LabVIEW codes run faster than Matlab codes. Moreover, it is indicated in [23] that classical engineering calculations (such as the Fast Fourier transform (FFT), which is important in OFDM systems) are very well optimized in LabVIEW and run faster than in MATLAB. Furthermore, compared with MATLAB, LabVIEW provides a simplified integration with hardware so we can quickly acquire and virtually visualize data generated by NI and third-party input/output (I/O) devices, making it more convenient for generating and acquiring signals [23]. This leads to a rapid configuration with significantly reduced programming and debugging time [22], [24].

Due to these advantages of LabVIEW, the digital signal processing algorithms in the proposed system are written directly using LabVIEW to ensure a fast signal processing and convenient signal acquisition. Nevertheless, researchers can conveniently integrate the Matlab scripts of their algorithms into the proposed system, for example, in the form of LabVIEW MATLAB Script nodes. Hybrid programming where LabVIEW is used for generating and acquiring signals and MATLAB is applied to carry out complex computing combines merits of both tools to ensure a rapid real-time system development [22], [24], [25].

NI devices and LabVIEW have been used in [26]-[28] to implement UA modems. However, [26] and [27] did not consider OFDM systems. LabVIEW has been used in [28] to study the performance of peak-to-average power ratio reduction algorithms in UA OFDM systems. Compared with [28], our paper presents a more complete and more practical implementation of UA OFDM system in that (1) Carrier frequency offset estimation and compensation are essential parts of a practical UA OFDM system due to the large Doppler shift in UA channels. They have been implemented in our system, but not in [28]. (2) The subcarrier spacing in [28] is 21.5 Hz, which is much larger than the 7.8 Hz adopted in this paper. This may lead to a low system spectral efficiency. (3) Channel coding is important for a practical UA OFDM system, which has been implemented in our system, but not in [28]. (4) Block-type pilots are applied in [28], while in this paper comb-type pilots are adopted. It is well known that the latter one has a better performance in fast time-varying UA channels [29].

The performance of our UA OFDM system is verified through recent UA communication experiments performed in a tank, in the Canning River, and in the estuary of the Swan River, Western Australia. These three experiments are used to verify the performance of the proposed system step-by-step in three phases. A tank experiment is usually the first step in testing the performance of an underwater OFDM system in a multipath channel environment. Results of the tank experiment verify that basic system parameters such as the length of the cyclic prefix are correctly chosen. However, in the tank experiment, the proposed system is not subject to noise in a real underwater acoustic communication environment, which necessitates the river experiments. The Canning River experiment verifies the system performance under practical noise environment in a short communication distance. Finally, the Swan River experiment was carried out to study the performance of the system in a longer communication range. Experimental results demonstrate that the system achieves a reliable bit-error-rate (BER) performance even with high-order modulation schemes. Thus, our system can be used in various UA communication tasks such as establishing reliable communication links among nodes in a UA sensor network. Compared with [30], this paper provides more details on the system design and performance analysis including (1) The state machine diagrams of the transmitter and receiver. (2) More detailed transmitter flow chart and detailed receiver flowchart in the idle mode, the detection mode, and the decoding mode. (3) Algorithm implementation. (4) In [30], only results of the tank experiment were partly presented, while in this paper, we also present important results of two river experiments, which demonstrate the capability of our system in practical UA communication environments.

The remainder of this paper is organized as follows. The UA OFDM system model is presented in Section II. The system hardware and software implementations are presented in Section III and Section IV, respectively. The results of the tank and river experiments are demonstrated in Section V and Section VI, respectively. In Section VII, conclusions are drawn and future work is discussed.

II. System Model

We apply the NI LabVIEW software to design a frame-based coded UA OFDM communication system in this paper. The block diagram of the proposed transmitter system is illustrated in Fig. 1. It can be seen that for each data frame, the transmitter first generates a binary source data stream $\boldsymbol{b} = (b[1], \ldots, b[L_b])^T$, where L_b denotes the number of information-carrying bits in each data frame and $(\cdot)^T$ stands for the matrix (vector) transpose. This source bits stream is passed through a turbo encoder, interleaved, and (possibly) punctured to form a coded sequence $\boldsymbol{c} = (c[1], \ldots, c[L_c])^T$ of length $L_c = R_m N_s N_b$, where N_b is the number of OFDM blocks in one data frame, N_s is the number of data subcarriers, and R_m is the modulation order. The encoded sequence $\boldsymbol{c}$ is mapped by the modulation module into $N_s N_b$ data symbols drawn from either the PSK or the quadrature

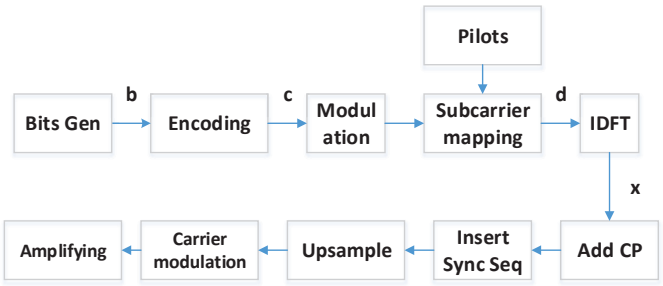

Fig. 1. Block diagram of the transmitter in a UA OFDM communication system.

amplitude modulation (QAM) constellations. Then every N_s data symbols together with N_p quadrature PSK (QPSK) modulated pilot symbols are mapped into corresponding subcarriers to form one OFDM symbol vector $\boldsymbol{d} = (d[1], \ldots, d[N_c])^T$, where N_c and N_p denote the number of total subcarriers and pilot subcarriers, respectively, with the pilot subcarriers being uniformly spaced. There are $N_0 = N_c - N_p - N_s$ null subcarriers in the system.

Using the inverse discrete Fourier transform (DFT), the OFDM symbol $\boldsymbol{d}$ is converted to the time domain, leading to an $N_c \times 1$ baseband discrete time signal vector given by

$$\boldsymbol{x} = \boldsymbol{F}^H \boldsymbol{d} \tag{1}$$

where $\boldsymbol{F}$ is an $N_c \times N_c$ DFT matrix with the (i,k)-th entry of $1/\sqrt{N_c} e^{-j2\pi(i-1)(k-1)/N_c}$, $i,k = 1, \ldots, N_c$, and $(\cdot)^H$ denotes the conjugate transpose. Then $\boldsymbol{x}$ is prepended by a cyclic prefix (CP) longer than the channel delay spread, followed by upsampling and upshifting operations. Let T_{cp} and f_{sc} denote the length of the CP and the subcarrier spacing, respectively. We can obtain that the length of one OFDM symbol is $T = 1/f_{sc}$, the total length of one OFDM block is $T_{total} = T + T_{cp}$, and the bandwidth of the transmitted signal is $B = f_{sc} N_c$. The upshifted samples are scaled by an amplifying factor α, which is used to control the power of the transmitted signals.

At the receiver side, we first perform the synchronization operation. Then after downshifting and low-pass filtering, we sample the received signal at a rate of B. After removing the CP, the baseband discrete time samples of one OFDM symbol is given by

$$\boldsymbol{r} = \boldsymbol{P}\boldsymbol{F}^H \boldsymbol{D}\boldsymbol{h}_f + \boldsymbol{w} = \boldsymbol{P}\boldsymbol{F}^H \boldsymbol{D}\boldsymbol{F}\boldsymbol{h}_t + \boldsymbol{w} \tag{2}$$

where $\boldsymbol{r} = (r[1], \ldots, r[N_c])^T$, $\boldsymbol{w} = (w[1], \ldots, w[N_c])^T$ is the noise samples, and $\boldsymbol{D} = \mathrm{diag}(\boldsymbol{d})$ is a diagonal matrix taking $\boldsymbol{d}$ as the main diagonal elements. In (2), $\boldsymbol{P} = \mathrm{diag}(\boldsymbol{p})$ with $\boldsymbol{p} = (1, e^{-j2\pi f_o/B}, \ldots, e^{-j2\pi(N_c-1)f_o/B})^T$ denotes the phase distortion introduced by the Doppler shift, f_o is the frequency offset, $\boldsymbol{h}_f = (h_f[1], \ldots, h_f[N_c])^T$ is the channel frequency response vector at all N_c subcarriers, and $\boldsymbol{h}_t = \boldsymbol{F}^H \boldsymbol{h}_f$ is the discrete time domain channel impulse response with a maximal delay of L_m.

After the frequency offset estimation and removing, the frequency domain received signal is given by

$$\begin{aligned} \boldsymbol{r}_f &= \boldsymbol{F}\boldsymbol{r} \\ &= \boldsymbol{F}\boldsymbol{F}^H \boldsymbol{D}\boldsymbol{h}_f + \boldsymbol{F}\boldsymbol{w} \\ &= \boldsymbol{D}\boldsymbol{h}_f + \boldsymbol{w}_f \end{aligned} \tag{3}$$

where $\boldsymbol{w}_f = \boldsymbol{F}\boldsymbol{w}$ is the frequency domain noise vector.

TABLE I
A LIST OF SYSTEM HARDWARE

Device Name	Device Function
NI cDAQ-9174	Transfer data between computer and I/O devices
NI-9232	Acquire signals from the hydrophone
NI-9260	Output signals to the transducer
CTG0052	Transmitter transducer
HTI-96-Min	Receiver hydrophone

III. SYSTEM HARDWARE IMPLEMENTATION

A list of system hardware and their functions in our UA OFDM system is shown in Table I. In particular, a NI CompactDAQ system is used for signal generation and acquisition in our UA OFDM communication system. CompactDAQ is a small modular data acquisition and measurement system capable of digital I/O, analog I/O, industrial bus communication, and counter/timer operations. The CompactDAQ system which we use in our system design consists of a chassis and two NI I/O modules as described below.

A. NI cDAQ-9174 Chassis

cDAQ-9174 is a plug-and-play chassis developed for small portable sensor measurement systems. Via a USB cable, it controls the synchronization, timing, and data transfer between an external host (e.g. desktop computer) and up to four I/O modules. Using this chassis, we can perform a mix of digital I/O, analog I/O, and counter/timer measurements. There are four 32-bit general-purpose counter/timers in cDAQ-9174. Using multiple timing engines, up to seven hardware-timed operations can be conducted simultaneously, with three independent rates for analog input.

B. NI-9232 Module

NI-9232 is a three-channel signal acquisition module. These three input channels can perform simultaneous signal measurement. Moreover, each channel has a maximal sampling rate of 102.4k samples/s and a built-in anti-aliasing filter which is automatically adjusted to the sampling rate. NI-9232 also provides software-selectable DC/AC coupling. Together with NI software, the NI-9232 module can execute signal processing functions such as order tracking and frequency analysis of the received signal. In our UA OFDM system, this module is plugged into the cDAQ-9174 chassis to acquire signals received from the hydrophone.

C. NI-9260 Module

NI-9260 is a two-channel voltage output module. It provides an update rate of 51.2k samples/s with a 24-bit resolution, 3 V output range, and 30 V over-voltage protection. In our UA OFDM system, this module is plugged into the cDAQ-9174 chassis to transmit signals to the transducer.

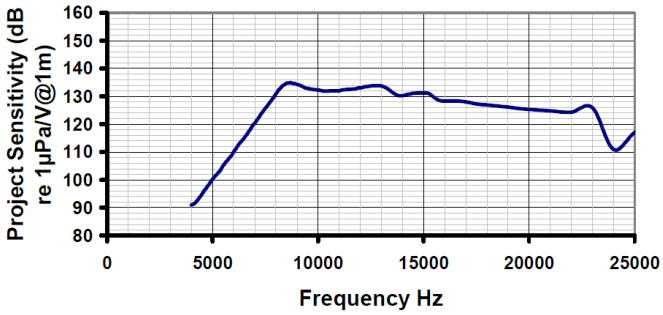

Fig. 2. Transmit sensitivity of the CTG0052 transducer.

D. CTG0052 Transducer

The CTG0052 UA transducer from Chelsea Technologies is a high power and low frequency transducer. The effective frequency range of this transducer is 8-16 kHz, which covers the spectrum of telephony, telemetry, and other underwater acoustic applications. The transmit sensitivity of the CTG0052 transducer is illustrated in Fig. 2. In our system design, the transducer is connected to the NI-9260 module through a transformer matching network and a power amplifier to transmit acoustic signals through the underwater channel.

E. HTI-96-Min Hydrophone

The HTI-96-Min exportable hydrophone from the High Tech Inc. is widely applied in UA communications. The sensitivity of this hydrophone is -201 dB re: 1V/μPa with a frequency range of 2 Hz-30 kHz. In our UA OFDM system, this hydrophone is connected to the NI-9232 module through a preamplifier to acquire signals received from the UA channel.

IV. System Transceiver Algorithms Design

The transceiver algorithms in our UA OFDM system is implemented by the NI LabVIEW software, which is an integrated graphical programming platform. In this section, we present in detail the implementation of the system software at both the transmitter side and the receiver side.

A. Overview of the Transmitter Software Design

The key parameters of the UA OFDM system are summarized in Table II. The system parameters are determined based on the following rationale. Firstly, the carrier frequency and bandwidth[1] are determined based on the sensitivity of the transducer in Fig. 2. Secondly, the length of the CP is set based on the maximal delay spread of the UA channel measured in the tank and river experiments to be presented later on. Thirdly, to achieve a high system efficiency, the length of one OFDM symbol should be much longer than the length of the CP. This together with the fact that the number of subcarriers is power of 2 to enable FFT, we choose $N_c = 512$. Then f_{sc} and T in Table II can be calculated based on the value of B and N_c.

[1]For UA waves, attenuation due to absorption increases rapidly with increasing frequency. Thus, the effective bandwidth and carrier frequency of a UA communication system is inversely proportional to the transmission distance. In general, the system architecture and approaches presented in this paper are applicable to UA OFDM systems operating at other frequency bands.

TABLE II
UA OFDM System Parameters

Carrier frequency	f_c	12 kHz
Sampling rate	T_s	48 kHz
Bandwidth	B	4 kHz
Number of subcarriers	N_c	512
Subcarrier spacing	f_{sc}	7.8 Hz
Length of OFDM symbol	T	128 ms
Length of CP	T_{cp}	25 ms

Fig. 3. Data frame structure of the transmitted signals.

Fig. 3 illustrates the data frame structure of the transmitted signals. We can see from Fig. 3 that each data frame contains one preamble block and $N_b = 5$ OFDM data blocks. This frame structure is determined by considering both the system efficiency and the variability of the UA channel. The preamble block is used for the purpose of synchronization and frame head detection, which consists of an $N_{pn} = 127$ long pseudo noise (PN) sequence followed by N_{pn} zeros. Among the $N_c = 512$ subcarriers, there are $N_s = 325$ data subcarriers and $N_p = 128$ uniformly spaced pilot subcarriers while the remaining $N_0 = 59$ subcarriers are used for the carrier frequency offset estimation. Note that the pilot subcarrier spacing is determined based on the maximal delay spread of the UA channel measured in the tank and river experiments. The data symbols are modulated by either QPSK or 16-QAM constellations encoded by 1/3 rate turbo codes. In each data frame, the number of information-carrying bits is $L_b = 1088$ for the QPSK modulation and $L_b = 2176$ for the 16-QAM modulation scheme.

The state machine diagram describing the working states of the transmitter is illustrated in Fig. 4. After the initialization of the transmitter system, it enters the idle state and remains in the idle state until it receives instruction to transmit a new data frame. The transmitter returns to the idle state automatically at the end of the transmission mode processing.

The flowchart of the signal processing in the idle and transmission modes is shown in Fig. 5. In the idle mode, the system first clears the frame counter if necessary. Then the transmitter checks the status of the reset button (see Fig. 13) and resets the system parameters (including the length

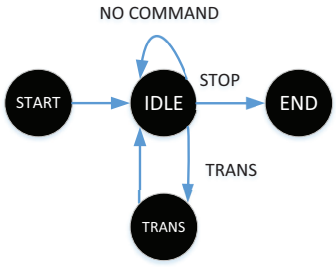

Fig. 4. The state machine diagram of the transmitter.

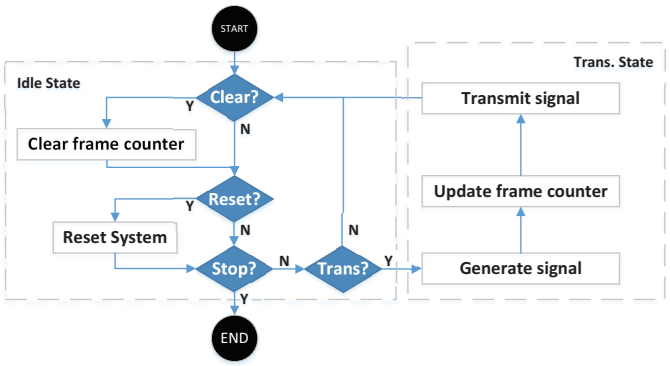

Fig. 5. Transmitter flowchart.

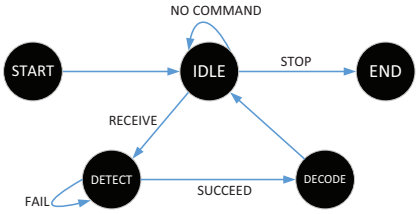

Fig. 6. The state machine diagram of the receiver.

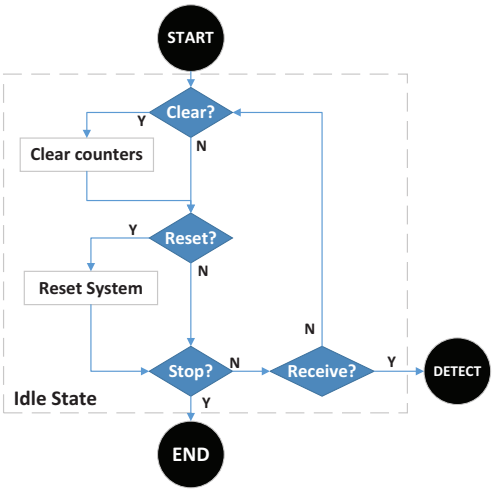

Fig. 7. Receiver idle mode flowchart.

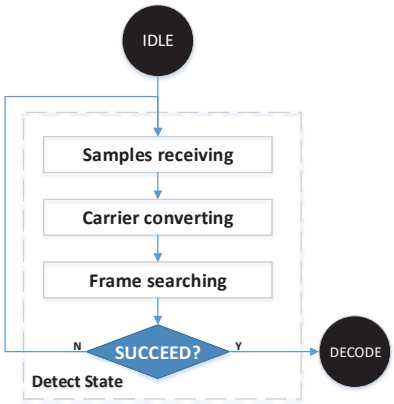

Fig. 8. Receiver detection mode flowchart.

of the preamble block, the modulation type, the source bits and the parameters for the turbo encoder) if required. After this operation, the transmitter checks the status of the stop button (see Fig. 13) and stops running if instructed. Otherwise, the transmitter checks the status of the transmission button (see Fig. 13) and enters the transmission mode if required. Otherwise, the transmitter stays in the idle state and starts the next round of checking if no transmission is instructed.

In the transmission state, the system first generates one data frame based on the procedure in Fig. 1. Then, the transmitter forwards the generated data to the NI-9260 module, increases the frame counter by one, and and then returns to the idle state.

B. Overview of the Receiver Software Design

The state machine diagram describing the working states of the receiver is shown in Fig. 6. After the initialization of the receiver system, it enters the idle state and remains in this state until further instruction is given to the system. The system stops running once the stop command (see Fig. 14) is received. Otherwise, the system enters the detection mode if it is required to process a received frame. In the detection mode, the receiver searches the frame head and remains in this mode if it fails to detect the frame head. Otherwise, the system enters the decoding state where the frame payload is received and processed. The receiver returns to the idle state at the end of the decoding processing.

The flowchart of the signal processing at the receiver in the idle mode is shown in Fig. 7. The receiver first clears the counters if necessary. Then the receiver resets the system parameters (including the preamble, the modulation type, and the parameters for the turbo decoder) if necessary. Then the receiver checks the status of the stop button (see Fig. 14) and stops running if instructed. Otherwise, the status of the receiving button (see Fig. 14) is checked. The receiver stays in the idle state and starts the next round of checking, if the system is not instructed to receive signals. Otherwise, the receiver enters the detection mode.

The flowchart of the data processing in the detection mode is shown in Fig. 8. In this mode, signal samples received from the NI-9232 module are first shifted from the passband to the baseband. Then the system uses the baseband signals and the local synchronization sequence to detect the frame head. After the synchronization sequence is successfully detected, the receiver enters the decoding mode whose flowchart is illustrated in Fig. 9. The receiver first downshifts and downsamples the samples received by the NI-9232 module. Then the CP is removed from every received OFDM block. The receiver then processes the received baseband signals to obtain the decoded bits as discussed later. The decoded bits are compared with the original transmitted bit sequence to determine the receiver performance. Various counters are updated including the detected frame counter, the successfully decoded frame counter, and the erroneous bit counter. Finally, the receiver returns to the idle state again.

The block diagram of the baseband signal processing at the receiver side is illustrated in Fig. 10. We can see that for each

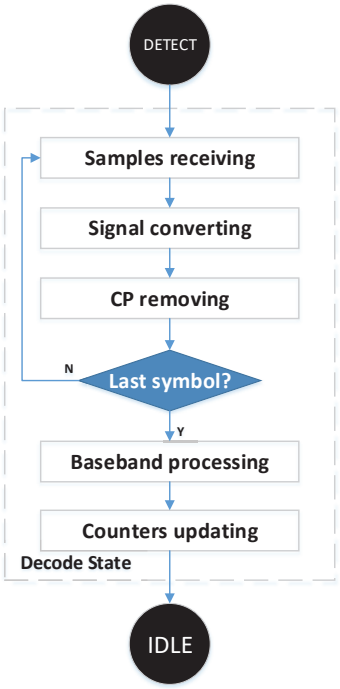

Fig. 9. Receiver decoding flowchart.

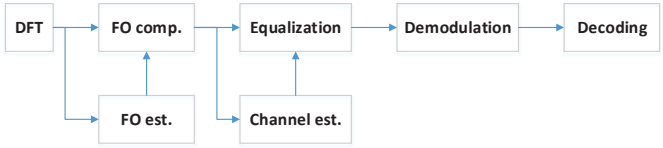

Fig. 10. Block diagram of the baseband signal processing at the receiver.

OFDM symbol, the receiver first performs carrier frequency offset estimation and compensation by exploiting the null subcarriers. Then the baseband signals are processed by the channel estimation block, which applies the least-squares (LS) approach to estimate the channel frequency response using the pilot subcarriers. The channel estimator then applies the linear interpolation to obtain the channel responses of the data subcarriers based on the channel responses at the pilot subcarriers. Channel equalization is performed on the received signals using the estimated channel response. After this, the receiver demodulates the equalized data to obtain a raw bit sequence. Finally, the raw bit sequence is processed by a turbo decoder.

C. Algorithm Implementation

1) Carrier downshifting: This process moves the received signals from the passband to the baseband at the receiver. In particular, the received samples are first passed through a passband filter, which is a 300th order pre-defined filter with a sampling rate of 48 kHz and passband from 9 kHz to 14 kHz. Then a carrier signal of 12 kHz is generated and used to remove the carrier frequency of the filtered signal. Finally, the signals are passed through a 600th order lowpass filter with a sampling rate of 48 kHz and a stop frequency of 2.2 kHz.

2) Frame head searching: DFT-based cross-correlation between the received samples and the local synchronization sequence is calculated to detect the frame head through a sliding window mechanism. In each attempt, the system appends N_{pn} samples received in the current attempt to the end of the N_{pn} samples received in the previous attempt, leading to a $2N_{pn}$-long sequence. This sequence goes through a $(2N_{pn}+2)$-point FFT and the result is multiplied with the FFT of the local synchronization sequence, followed by a $(2N_{pn}+2)$-point inverse FFT (IFFT). The system then calculates the average energy of the IFFT output and also finds the point with the maximal energy. If the quotient of the maximum energy over the average energy is larger than a preset threshold and the position of the maximal energy point is within the first N_{pn} samples, the system takes this position as the frame head. Otherwise, the system starts the next attempt.

3) Carrier frequency offset compensation: The Doppler shift compensation algorithm used in [17] is adopted here to estimate and compensate the carrier frequency offset. In the idle state, when the system is required to reset the system parameters, it calculates the tentative frequency offset points according to the settings and generates a length $N_c = 512$ phase rotation sequence for each point. For each tentative frequency point, the system compensates the frequency offset on the received OFDM symbol using the corresponding phase rotation sequence and then calculates the average energy of the null subcarriers. The system compares the average energy results generated by all tentative frequency points and chooses the frequency point with the lowest average energy. The phase rotation sequence associated with this frequency point is used to compensate the frequency offset.

4) Turbo coding: The turbo coding algorithm defined in [31] is adopted here for channel coding. Note that to reduce the computation time at the transmitter and receiver, the turbo encoder and decoder are implemented by the C Language and embedded at the transmitter and the receiver, respectively, through the dynamic-link library (DLL) technique.

V. Results of the Tank Experiment

In this section, we investigate the performance of our LabVIEW and CompactDAQ-based UA OFDM system in a multipath channel environment through a tank experiment. The setup of the experimental system is illustrated in Fig. 11. It can be seen that the NI cDAQ-9174 chassis is connected to a host computer via a USB cable. The NI LabVIEW software is installed on the computer for the signal generation and processing. The NI-9260 and NI-9232 modules are plugged into slot 2 and slot 1 of the cDAQ-9174 chassis, respectively. The CTG0052 UA transducer is connected through a power amplifier and matching network to channel 1 of the NI-9260 module for transmitting UA communication signals. Channel 0 of the NI-9232 module is connected through a preamplifier to the HTI-96-Min hydrophone for receiving the UA communication signals. The hydrophone and the transducer are placed in a rectangular tank with a length of 2.5 m and a width of 1.5 m. The water depth was 1.8 m during the experiment (see Table III). Fig. 12 shows the locations of the

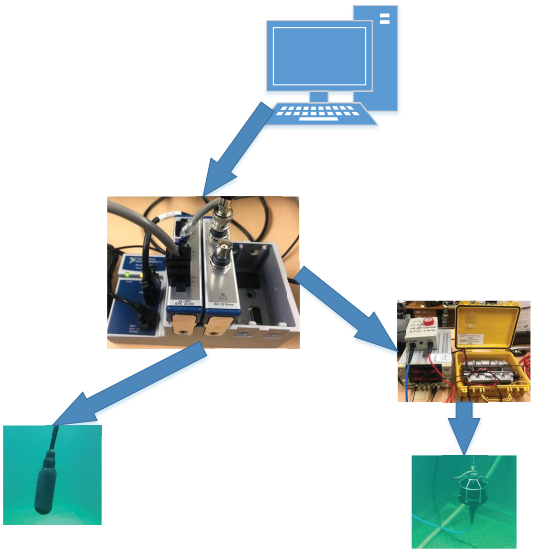

Fig. 11. Experimental system setup.

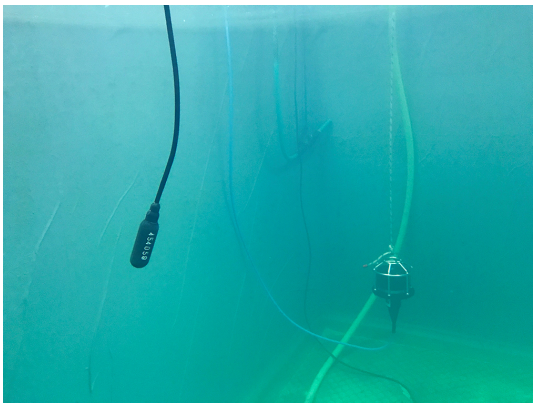

Fig. 12. Locations of the transducer and hydrophone in the tank.

hydrophone (left) and the transducer (right) in the tank. As the Doppler shift is negligible in a tank environment, the frequency offset estimation and compensation modules in Fig. 10 were bypassed during the tank experiment.

Fig. 13 illustrates the signal spectrum and waveform of several transmitted data frames. Fig. 14 shows the waveforms of the passband signals and baseband signals with/without oversampling in one successfully detected data frame. The amplitude of the cross-correlation between the local synchronization sequence and the received preamble block is also illustrated in Fig. 14.

The frequency domain amplitudes of the passband and baseband signals of the first received OFDM symbol in a successfully decoded data frame are illustrated in Fig. 15, together with the scatter plots of the received symbols before

TABLE III
EXPERIMENTAL SETUP

Location	Distance	Water depth	Modulation
Tank	2.5 m	1.8 m	QPSK
Canning River	10 m	1.5 m	16-QAM
Swan River	936 m	2.5 m $\sim$ 6 m	QPSK

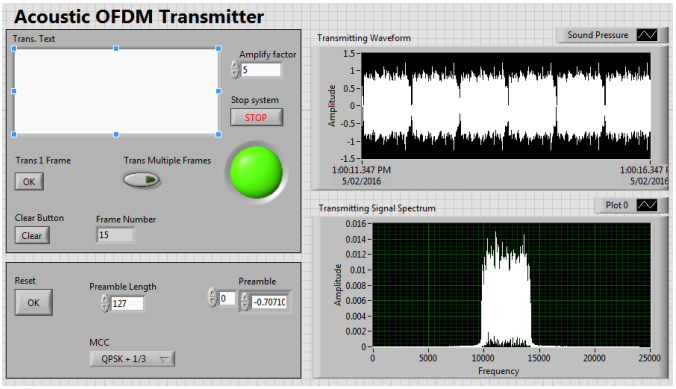

Fig. 13. Signal waveform and spectrum of several transmitted data frames.

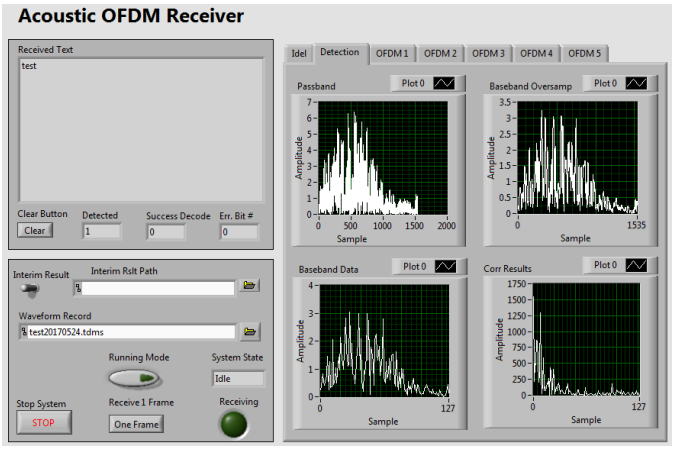

Fig. 14. A successfully detected data frame with the QPSK modulation scheme.

and after the channel equalization. We can observe from Fig. 15 that a majority of the symbols are correctly aggregated into the normalized QPSK constellations after the channel equalization.

Fig. 16 shows the power of the channel impulse response during the tank experiment estimated by the pilot subcarriers. We can observe from Fig. 16 that the maximal channel delay spread in the experiment is about 15 ms which is shorter than

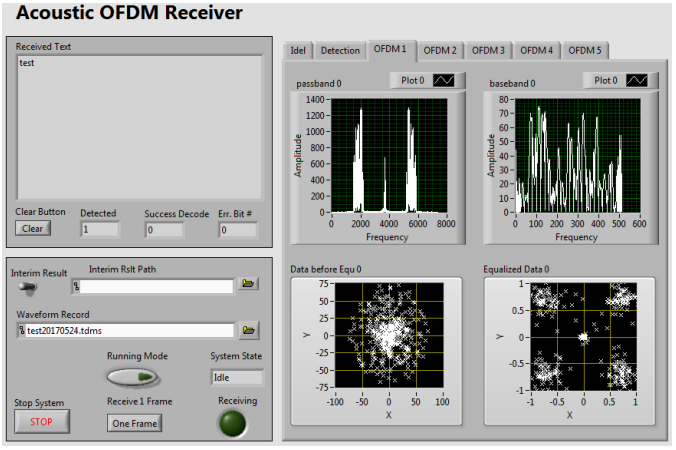

Fig. 15. A received OFDM block with the QPSK modulation scheme.

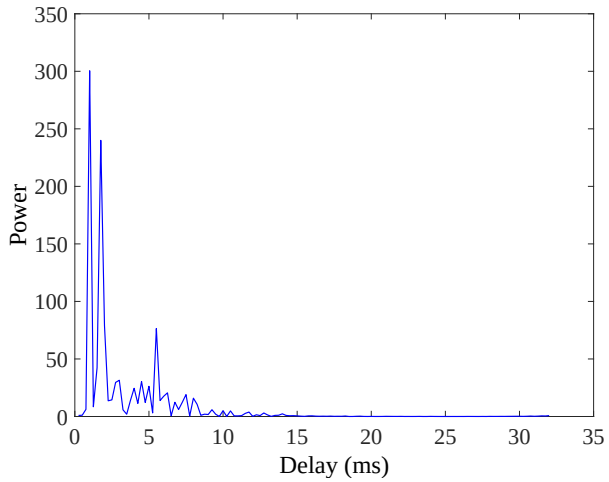

Fig. 16. Power of the channel impulse response estimated by the pilot subcarriers during the tank experiment.

the length of the CP. Interestingly, it can be seen that there are many notable paths between the transmitter and the receiver due to multiple reflections of the acoustic signals off the walls of the tank. As the pilot subcarriers can estimate multipath channels with a delay spread up to 32 ms, this verifies the system parameters such as the length of the CP and the pilot subcarrier spacing are correctly chosen. Results of the tank experiment also indicate that our system is sufficiently fast to complete processing one data frame before the end of the next data frame in a continuous fashion.

VI. Results of the River Experiment

Another UA communication experiment using the system we developed was conducted in October 2017, in the Canning River, Western Australia, to test the performance of the system in real underwater acoustic communication environment. Canning River has brackish water with varying salinity. The water depth was approximately 1.5 m. A single hydrophone at the receiver was attached through a cable at around half a meter above the river bed, while a transducer attached through a cable was located also about half a meter above the river bed. The distance between the hydrophone and the transducer was around 10 m. To evaluate the system performance, The OFDM signals were transmitted at various power levels by modifying the amplification factor α.

The amplitude of the received signals and the background noise at various levels of α is shown in Fig. 17. It can be seen that at $\alpha = 5 \times 10^{-4}$, the amplitude of the received signals is comparable to that of the background noise, which is highly impulsive. A typical channel impulse response during the river experiment estimated by the pilot subcarriers is shown in Fig. 18. It can be seen from Figs. 16 and 18 that the number of notable paths between the transmitter and the receiver and the maximal channel delay spread are usually larger in a tank experiment compared with those in real environments such as rivers. Therefore, the results obtained in the tank experiment provide a reliable guideline in choosing system parameters such as the length of the CP and the pilot subcarrier spacing.

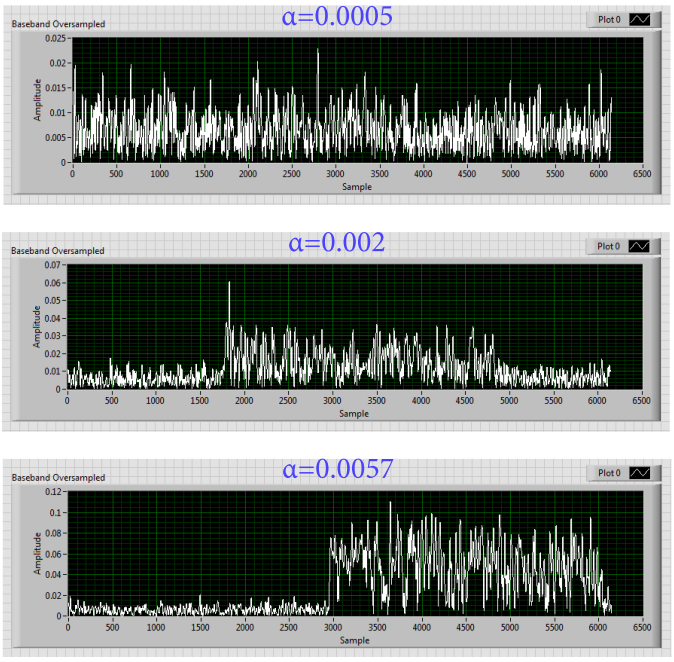

Fig. 17. Amplitude of the received signals and the background noise at various α.

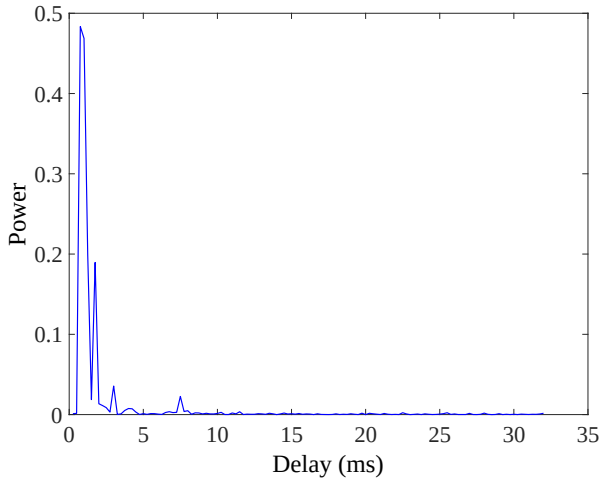

Fig. 18. Power of the channel impulse response estimated by the pilot subcarriers during the Canning River experiment.

Fig. 19 illustrates the waveforms of the passband signals and baseband signals with/without oversampling in one successfully detected data frame. The amplitude of the cross-correlation between the received preamble block and the local synchronization sequence is also shown in Fig. 19. Fig. 20 shows the frequency domain amplitudes of the passband and baseband signals of the fourth received OFDM symbol in a successfully decoded data frame using the 16-QAM modulation. We can observe that after the channel equalization, a majority of the received symbols are correctly aggregated into the normalized 16-QAM modulation constellations.

To evaluate the BER and block-error-rate (BLER) performance of the system we developed, we varied the transmission

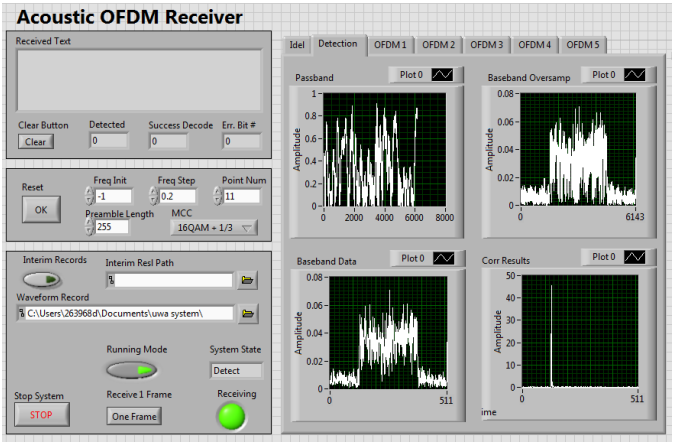

Fig. 19. A successfully detected data frame with the 16-QAM modulation scheme.

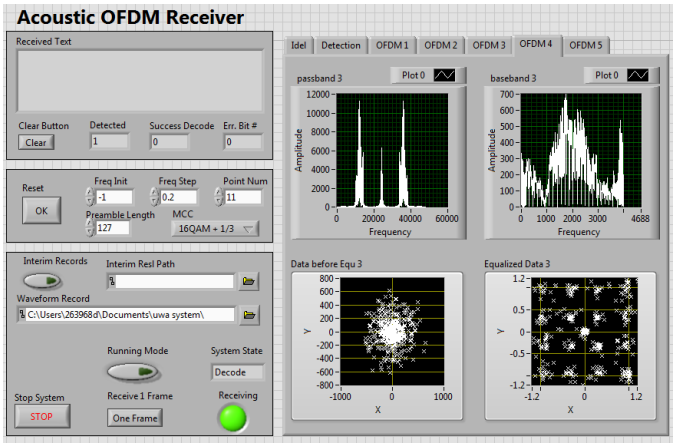

Fig. 20. A received OFDM block with the 16-QAM modulation scheme.

power through adjusting the amplification factor α. In particular, we set α to 0.0020, 0.0024, 0.0028, 0.0034, 0.0040, and 0.0057, respectively. For each α, 300 data blocks were transmitted during the experiment, and the BER is obtained for bits in these 300 blocks. To calculate the BLER, one received block is considered erroneous if one or more of the information-carrying bits in this block is incorrectly decoded. The BER and BLER performance of the detected frames are shown in Fig. 21 for the 16-QAM constellations. In order to correlate α with the signal-to-noise ratio (SNR) at the receiver, which is commonly used to study the BER performance of a communication system, we estimate the SNR from the received data. The estimated SNRs at the receiver associated with various α are shown in Table IV. Interestingly, it can be seen from Table IV that although based on the values of α, there is a difference of 1.5 dB in the power levels between two adjacent transmissions except for the last one which is around a 3 dB change, the difference of SNRs between two adjacent transmissions varies between 0.2 dB and 2.3 dB. The reason is that the SNR is strongly affected by the presence of highly sparse and time-varying impulsive noise in the received signals.

To further study the performance of the proposed LabVIEW

TABLE IV
ESTIMATED SNR AT THE RECEIVER ASSOCIATED WITH VARIOUS α

α	Estimated SNR (dB)
0.002	4.84
0.0024	5.04
0.0028	7.30
0.0034	7.92
0.004	8.40
0.0057	10.04

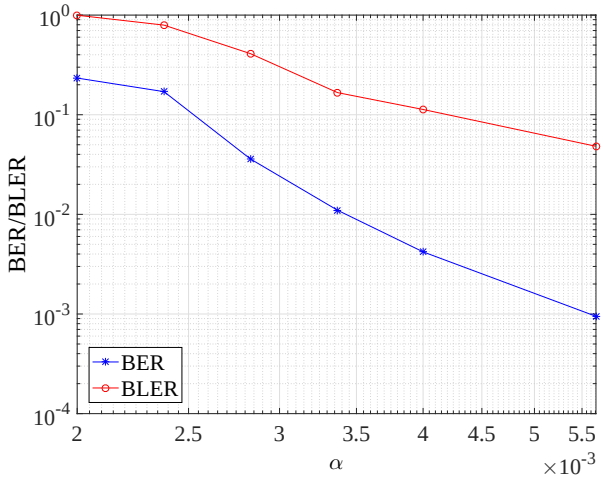

Fig. 21. BER/BLER versus α for 16-QAM signals.

and CompactDAQ-based UA OFDM system in a longer communication distance, we apply this system to decode the data recorded during a UA communication experiment conducted in the estuary of the Swan River, Western Australia. The locations of the transmitter transducer and the receiver hydrophone are shown in Fig. 22, where the distance between the transmitter and the receiver was around 936 m. The water depth along the direct path varied between 2.5 m and 6 m. Both the transmitter transducer and the receiver hydrophone were mounted 0.5 m above the river bed on steel frames and were cabled to shore. The water depths at the transmitter and the receiver were 5 m and 2.5 m, respectively. The same data file was transmitted three times during the day under different wave conditions. The data files recorded at the receiver during three

Fig. 22. Transmitter and receiver locations during the experiment.

TABLE V
BER AND BLER RESULTS OF THE SWAN RIVER EXPERIMENT

File	SNR (dB)	SIR (dB)	BER	BLER
T83	10.2	-8.0	0	0
T84	5.4	-13.1	8.3%	38.4%
T85	8.3	-13.3	1.1%	4.4%

TABLE VI
PERFORMANCE COMPARISON BETWEEN THE PROPOSED AND GPP BASED SYSTEMS IN [20]

System	Rate	Bandwidth	SE (b/s/Hz)	Distance
Proposed	2.63 kb/s	4 kHz	0.66	1 km
FAST	100 – 600 b/s	2 kHz	0.05 – 0.3	6 m
UCAC	4 – 80 b/s	3.5 kHz	0.001 – 0.02	20 km
RACUN	205 b/s	4 kHz	0.05	N/A

transmissions were named T83, T84, and T85, respectively. Each of the T83, T84, and T85 files contains 250 data frames in Fig. 3. Table V shows the BER and BLER of the proposed system using the QPSK modulation at various estimated SNR and estimated signal-to-impulsive noise ratio (SIR) levels. The SIR is introduced to measure the intensity of impulsive noise. As the hydrophone was located close to a jetty, there was a significant amount of impulsive noise from waves breaking at the jetty piers.

It can be seen from Table V that with a high SNR and SIR (the T83 file), the proposed system has zero BER and BLER for the data investigated. For a scenario with low SNR and SIR as the T84 file, our system achieves a BER of 8.3% and a BLER of 38.4%. With a medium SNR (the T85 file), the proposed system yields a BER of 1.1% and a BLER of 4.4%. These results correlate well with the wave conditions during the experiment. Indeed, we observed that the waves were low when the T83 file was recorded, and there were higher waves during the recoding of the T84 file. Results of the Swan River experiment also indicate that our system is sufficiently fast to complete processing one data frame before the end of the next data frame in a continuous fashion. As our system is running on open-architecture GPPs, the processing speed and capability required for UA communication can be easily satisfied by modern GPPs.

The performance comparison between the proposed LabVIEW based system and three GPP based systems in [20] in terms of data rate, system bandwidth, spectral efficiency (SE), and transmission distance is shown in Table VI. It can be seen from Table VI that the proposed system has a higher data rate and spectral efficiency.

VII. CONCLUSIONS AND FUTURE WORK

In this paper, a NI LabVIEW and CompactDAQ-based UA OFDM system design has been proposed. Details on the system hardware and software design have been presented. Baseband signal processing algorithms at the transmitter and receiver have been discussed. Tests in tank and river have been performed to verify the performance of the system developed. In the future, we will apply advanced channel estimation and impulsive noise mitigation techniques to improve the system performance. We also plan to use a NI cRIO to create a stand-alone UA OFDM system.

ACKNOWLEDGEMENT

The authors would like to thank the editor and anonymous reviewers for their valuable comments and suggestions that helped improve the quality of the paper.

REFERENCES

[1] D. Kilfoyle and A. Baggeroer, "The state of the art in underwater acoustic telemetry," *IEEE J. Ocean. Eng.*, vol. 25, no. 1, pp. 4-27, Jan. 2000.

[2] M. Chitre, S. H. Ong, and J. Potter, "Performance of coded OFDM in very shallow water channels and snapping shrimp noise," in *Proc. MTS/IEEE OCEANS*, Washington, DC, Sep. 2005, pp. 996–1001.

[3] B. Li, S. Zhou, M. Stojanovic, and L. Freitag, "Pilot-tone based ZP-OFDM demodulation for an underwater acoustic channel," in *Proc. MTS/IEEE OCEANS*, Boston, MA, Sep. 2006.

[4] B. Li, S. Zhou, M. Stojanovic, L. Freitag, and P. Willett, "Multicarrier communication over underwater acoustic channels with nonuniform Doppler shifts," *IEEE J. Ocean. Eng.*, vol. 33, no. 2, pp. 198-209, Apr. 2008.

[5] L. Wan, Z. Wang, S. Zhou, T. C. Yang, and Z. Shi, "Performance comparison of Doppler scale estimation methods for underwater acoustic OFDM," *Journal of Electrical and Computer Engineering*, vol. 2012, Artical ID 703243, 11 pages.

[6] Z. Wang, S. Zhou, J. Catipovic, and P. Willett, "Asynchronous multiuser reception for OFDM in underwater acoustic communications," *IEEE Trans. Wireless Commun.*, vol. 12, no. 3, pp. 1050-1061, Mar. 2013.

[7] P. Chen, Y. Rong, and S. Nordholm, "Pilot-subcarrier based impulsive noise mitigation for underwater acoustic OFDM systems," in *Proc. WUWNet 2016*, Shanghai, China, Oct. 24-26, 2016.

[8] P. Chen, Y. Rong, S. Nordholm, Z. He, and A. Duncan, "Joint channel estimation and impulsive noise mitigation in underwater acoustic OFDM communication systems," *IEEE Trans. Wireless Commun.*, vol. 16, no. 9, pp. 6165-6178, Sep. 2017.

[9] P. Chen, Y. Rong, S. Nordholm, and Z. He, "Joint channel and impulsive noise estimation in underwater acoustic OFDM systems," *IEEE Trans. Veh. Technol.*, vol. 66, no. 11, pp. 10567-10571, Nov. 2017.

[10] J. Wills, W. Ye, and J. Heidemann, "Low-power acoustic modem for dense underwater sensor networks," in *Proc. WUWNet*, Los Angeles, CA, Sep. 2006.

[11] B. Benson, G. Chang, D. Manov, B. Graham, and R. Kastner, "Design of a low-cost acoustic modem for moored oceanographic applications," in *Proc. WUWNet*, Los Angeles, CA, Sep. 2006.

[12] T. Fu, D. Doonan, C. Utley, R. Iltis, R. Kastner, and H. Lee, "Design and development of a software-defined underwater acoustic modem for sensor networks for environmental and ecological research," in *Proc. MTS/IEEE OCEANS*, Singapore, Sep. 2006.

[13] L. Freitag, M. Grund, S. Singh, J. Partan, P. Koski, and K. Ball, "The WHOI micro-modem: An acoustic communications and navigation system for multiple platforms," in *Proc. MTS/IEEE OCEANS*, Washington, DC, 2005.

[14] E. Sozer and M. Stojanovic, "Reconfigurable acoustic modem for underwater sensor networks," in *Proc. First ACM Int. Workshop Underwater Networks*, Los Angeles, CA, Sep. 2006.

[15] M. Aydinlink, A. Turan Ozdemir, and M. Stojanovic, "A physical layer implementation on reconfigurable underwater acoustic modem," in *Proc. MTS/IEEE OCEANS*, Quebec City, Canada, Sep. 2008.

[16] Z. Yan, J. Huang, and C. He, "Implementation of an OFDM underwater acoustic communication system on an underwater vehicle with multi-processor structure," *Frontiers of Electrical and Electronic Engineering in China*, vol. 2, no. 2, pp. 151-155, 2007.

[17] H. Yan, L. Wan, S. Zhou, Z. Shi, J. H. Cui, J. Huang, and H. Zhou, "DSP based receiver implementation for OFDM acoustic modems," *Phys. Commun.*, vol. 5, no. 1, pp. 22-32, 2012.

[18] G. Cario, A. Casavola, M. Lupia, and C. Rosace, "SeaModem: A low-cost underwater acoustic modem for shallow water communication," in *Proc. MTS/IEEE OCEANS*, Genova, Italy, May 2015.

[19] E. Demirors and T. Melodia, "SEANet G3: High-data-rate software-defined underwater acoustic network platform," in *Proc. UComms*, Lerici, Italy, Sep. 2016.

[20] H. S. Dol, P. Casari, T. van der Zwan, and R. Otnes, "Software-defined underwater acoustic modems: Historical review and the NILUS approach," *IEEE J. Ocean. Eng.*, vol. 42, no. 3, pp. 722-737, Jul. 2017.

[21] R. Gutiérrez-Castrejón and M. Duelk, "Using LabVIEW for advanced nonlinear optoelectronic device simulations in high-speed optical communications," *Comput. Phys. Commun.*, vol. 174, pp. 431-440, 2006.
[22] A. V. R. Kumar and K. R. Nataraj, "Result analysis of LabVIEW and MATLAB in application of image edge detection," *Int. J. Computer Applications*, vol. 48, no. 9, pp. 6-10, June 2012.
[23] T. Tašner, D. Lovrec, F. Tašner, and J. Edler, "Comparison of LabVIEW and MATLAB for scientific research," *Annuals of Faculty Engineering Hunedoara – International Journal of Engineering*, 2012.
[24] W. Xu, L. Zhong, and D. Wang, "Image processing based on seamless integration technology between LabVIEW and MATLAB," in *Proc. Int. Conf. Inform. Networking Automation*, Kunming, China, Oct. 17-19, 2010, vol. 1, pp. 219-223.
[25] J.-H. Horng, "Hybrid MATLAB and LabVIEW with neural network to implement a SCADA system of AC servo motor," *Advances in Engineering Software*, vol. 39, pp. 149-155, 2008.
[26] Y. Tao, P. Zhu, and X. Xu, "Dual-mode modulation based research of underwater acoustic modem," in *Proc. 6th Int. Conf. Wireless Commun., Networking and Mobile Computing*, Chengdu, China, Sep. 2010.
[27] P. Zhu, X. Xu, Y. Tao, and W. Wang, "The technology of underwater acoustic communication network nodes based on LabVIEW," *J. Xiamen University (Natural Science)*, vol. 49, no. 3, pp. 364-367, May. 2010.
[28] X. Xu, "Research on the PAPR reducing techniques in the OFDM underwater acoustic communication system," M.Eng. dissertation, Harbin Engineering University, China, 2007.
[29] S. Coleri, M. Ergen, A. Puri, and A. Bahai, "Channel estimation techniques based on pilot arrangement in OFDM systems," *IEEE Trans. Broadcasting*, vol. 48, no. 3, pp. 223-229, Sep. 2002.
[30] P. Chen, Y. Rong, S. Nordholm, A. Duncan, and Z. He, "A LabVIEW-based implementation of real-time underwater acoustic OFDM system," in *Proc. 23rd Asia-Pacific Conf. Commun.*, Perth, Australia, Dec. 11-13, 2017, pp. 730-734.
[31] LTE, "E-UTRA multiplexing and channel coding," TS 36.212 V12.2.0 Technical Specification, pp. 12-15, 2014.

PLACE PHOTO HERE

Peng Chen received the B.E. degree in Information Engineering and Ph.D. degree in Signal and Information Processing, both from Beijing University of Posts and Telecommunications, China, in 2007 and 2013, respectively. He was a System Engineer with Mobile Communication Division of Datang Mobile Communications Equipment Co., Ltd, Beijing, China, from April 2013 to September 2014. From October 2014 to November 2018, he was with the Department of Electrical and Computer Engineering, Curtin University, Bentley, Australia, as a Research Associate. His research interests include signal processing, wireless communication systems, algorithm design and channel estimation.

PLACE PHOTO HERE

Yue Rong (S'03-M'06-SM'11) received the Ph.D. degree (summa cum laude) in electrical engineering from the Darmstadt University of Technology, Darmstadt, Germany, in 2005. He was a Post-Doctoral Researcher with the Department of Electrical Engineering, University of California, Riverside, from February 2006 to November 2007. Since December 2007, he has been with the Department of Electrical and Computer Engineering, Curtin University, Bentley, Australia, where he is currently a full Professor. His research interests include signal processing for communications, wireless communications, underwater acoustic communications, applications of linear algebra and optimization methods, and statistical and array signal processing. He has published over 160 journal and conference papers in these areas.

Dr. Rong was a recipient of the Best Paper Award at the 2011 International Conference on Wireless Communications and Signal Processing, the Best Paper Award at the 2010 Asia-Pacific Conference on Communications, and the Young Researcher of the Year Award of the Faculty of Science and Engineering at Curtin University in 2010. He was an Associate Editor of the IEEE Transactions on Signal Processing from 2014 to 2018, an Editor of the IEEE Wireless Communications Letters from 2012 to 2014, a Guest Editor of the IEEE Journal on Selected Areas in Communications special issue on theories and methods for advanced wireless relays, and was a TPC Member for the IEEE ICC, IEEE GlobalSIP, EUSIPCO, IEEE ICCC, WCSP, IWCMC, and ChinaCom.

PLACE PHOTO HERE

Sven Nordholm (M'90-SM'05) received his Ph.D. in Signal Processing in 1992, Licentiate of engineering 1989 and MscEE (Civilingenjör) 1983 all from Lund University, Sweden. Since 1999, Nordholm is Professor Signal Processing, Department of Electrical and Computer Engineering, Curtin University. From 1999-2002, he was director of ATRI. From 2002-2009 he was director Signal Processing Laboratory, WATRI, Western Australian Telecommunication Research Institute, a joint institute between The University of Western Australia and Curtin University. He is a co-founder of a start-up companies; Sensear, providing voice communication in extreme noise conditions and Nuheara a hearables company. He is a Senior Member of IEEE, Associate Editor IEEE/ACM TASPL and a member of IEEE TC AASP.

His main research efforts have been spent in the fields of Speech Enhancement, Adaptive and Optimum Microphone Arrays, Audio Signal Processing and Acoustic Communication. He has written more than 200 papers in refereed journals and conference proceedings. He contributes frequently in book chapters and encyclopedia articles and is editor of two special issues on hearing aids and microphone arrays. He is holding 7 patents in the area of speech enhancement and microphone arrays.

PLACE PHOTO HERE

Zhiqiang He (S'01–M'04) received the B.E. degree in signal and information processing and the Ph.D. degree (Hons.) in signal and information processing from the Beijing University of Posts and Telecommunications (BUPT), Beijing, China, in 1999 and 2004, respectively. Since 2004, he has been with the School of Information and Communication Engineering, BUPT, where he is currently a Professor and the Director of the Center of Information Theory and Technology. His research interests include signal and information processing in wireless communications, networking architecture and protocol design, machine learning, and underwater acoustic communications.